Polymer Products Department for helpful suggestions and W. Mahler and R. C. Wheland for the preparation of some materials.

References and Notes

(1) C. A. Sperati and H. W. Starkweather, Jr., *Fortschr. Hochpolym.-Forsch.*, **2**, 400 (1961).
(2) N. K. J. Symons, *J. Polym. Sci.*, **51**, S21 (1961).
(3) C. A. Sperati in "Polymer Handbook", 2nd ed., J. Bandrup and E. H. Immergut, Eds., Wiley, New York, 1975, p V-29.
(4) J. D. Compton, J. W. Justice, and C. F. Irwin (to E. I. du Pont de Nemours and Co.), U. S. Patent 2 510 078, 1950.
(5) P. J. Flory, "Principles of Polymer Chemistry", Cornell University Press, Ithaca, NY, 1953, p 495.
(6) A Nakajima and F. Hamada, *Kolloid Z. Z. Polym.*, **205**, 55 (1965).
(7) P. J. Flory, R. A. Orwoll, and A. Vrij, *J. Am. Chem. Soc.*, **86**, 3515 (1964).
(8) P. J. Flory, A. Ciferri, and R. Chiang, *J. Am. Chem. Soc.*, **83**, 1023 (1961).
(9) P. Smith and R. St. John Manley, *Macromolecules*, **12**, 483 (1979).
(10) C. M. Cormier and B. Wunderlich, *J. Polym. Sci., Part A-2*, **4**, 666 (1966).
(11) T. Nishi and T. T. Wang, *Macromolecules*, **8**, 909 (1975).
(12) H. W. Starkweather, Jr., P. Zoller, G. A. Jones, and A. J. Vega, *J. Polym. Sci., Polym. Phys. Ed.*, **20**, 751 (1982).
(13) H. W. Starkweather, Jr., in preparation.
(14) B. Wunderlich, "Macromolecular Physics", Vol. 3, Academic Press, New York, 1980, p 87.
(15) M. Rothe in ref 4, p VI-4.
(16) A. P. Kudchadker, G. H. Alami, and B. J. Zwolinski, *Chem. Rev.*, **68**, 659 (1968).
(17) H. W. Starkweather, Jr., *Macromolecules*, **10**, 1161 (1977).
(18) P. J. Flory, *J. Chem. Phys.*, **17**, 223 (1949).
(19) P. Smith, Thesis, State University of Groningen, Groningen, 1976.
(20) R. R. Matheson, Jr., and P. Smith, *Polymer*, **26**, 288 (1985).
(21) P. Smith, unpublished results.
(22) A. J. Pennings and A. M. Kiel, *Kolloid Z. Z. Polym.*, **205**, 160 (1965).
(23) H. B. Hass and R. F. Newton in "Handbook of Chemistry and Physics", 53rd ed., R. C. Weast, Ed., The Chemical Rubber Publishing Co., Cleveland, OH, 1973, p D-144.
(24) R. L. Scott, *J. Phys. Chem.*, **62**, 136 (1958).
(25) "Handbook of Chemistry and Physics", CRC Press, Cleveland, OH.
(26) Reference 14, p 114.
(27) T. Suwa, M. Takehisa, and S. Machi, *J. Appl. Polym. Sci.*, **17**, 3253 (1973).
(28) A. D. English and O. T. Garza, *Macromolecules*, **12**, 351 (1979).

Simulation of Upper and Lower Critical Phase Diagrams for Polymer Mixtures at Various Pressures

Shamsedin Rostami and David J. Walsh*

Department of Chemical Engineering and Chemical Technology, Imperial College, London SW7, United Kingdom. *Received September 27, 1984*

ABSTRACT: A procedure is described for the simultaneous prediction of the binodal and spinodal curves of polymer mixtures at various pressures using a form of the equation-of-state theory of Flory and co-workers. The results of the calculation are compared with experimental results for the effect of pressure on the cloud points of both oligomer mixtures showing upper critical behavior and polymer mixtures showing lower critical behavior. The procedure successfully predicts the sign of the effect and its magnitude within the experimental and theoretical uncertainties for the systems studied.

Introduction

The equation-of-state theory of Flory and co-workers[1-4] has been widely used in describing the miscibility of polymer or oligomer mixtures. The ability of the theory to predict both upper critical solution temperature (UCST) and lower critical solution temperature (LCST) phase diagrams has been demonstrated by several authors.[5-7]

The effect of pressure on the miscibility of polymer–solvent mixtures and oligomer mixtures has been experimentally studied.[10-12] We have also studied the effect of pressure on the miscibility of polymer–polymer blends showing LCST behavior.[13] These studies have shown the following:

(a) For mixtures showing UCST behavior with negative heats of mixing the application of pressure causes the temperature range of miscibility to increase whereas for those with positive heats of mixing the temperature range of miscibility decreases.

(b) For high molecular mass polymer blends showing LCST behavior the effect of pressure increases the temperature range of miscibility.

In this paper we deal with the effect of pressure on both oligomer mixtures showing UCST behavior and high-polymer mixtures showing LCST behavior. Experimental results were obtained for samples of blends held in a pressure bomb and examined by measurement of turbidity during temperature scans. The apparatus, technique, and experimental results are described elsewhere.[11,13]

The theoretical procedure involves obtaining values of the hard-core pressure, volume, and temperature (P^*, V^*, and T^*) of the components from known physical data and a value of the contact interaction parameter, X_{12}, from heat of mixing measurements using oligomeric mixtures. The noncombinatorial contact parameter, Q_{12}, is then used as the only adjustable parameter to fit the minimum of the phase diagram to that of the experimental cloud point curve at atmospheric pressure. This value is then used to calculate the spinodal and binodal curves over the whole range of composition and pressure. The procedure used to calculate the binodal and spinodal curves has been described elsewhere[6-9,13] and will only be described briefly here. It should be pointed out that the assumption that both X_{12} and Q_{12} are independent of both temperature and pressure can only be approximate. Both temperature and pressure may change the interaction energies. Pressure may also cause configurational changes in molecules, an effect which has been found to be greatest for shorter chain lengths.[14]

Theory

To obtain the effect of pressure on the phase diagram of mixtures the hard-core properties of the pure compo-

0024-9297/85/2218-1228$01.50/0

nents, T^*, P^*, and V^*, were computed from the thermal expansion coefficient, α, thermal pressure coefficient, γ, and density, d, of the corresponding material using the following equations.[1-4] The notation is given in the Appendix.

$$\tilde{v}_i = \left[1 + \frac{\alpha_i T}{3 + 3\alpha_i T} \right]^3 \tag{1a}$$

$$V_i^* = M_i/(d_i \tilde{v}_i) \tag{1b}$$

$$P_i^* = \gamma_i T \tilde{v}_i^2 \tag{2}$$

$$T_i^* = T\tilde{v}_i^{3/4}/(\tilde{v}_i^{4/3} - 1) \tag{3}$$

The hard-core characteristic pressure, P^*, and temperature, T^*, of the mixture are given by

$$P^* = \phi_1 P_1^* + \phi_2 P_2^* - \phi_1\theta_2 X_{12} \tag{4}$$

$$R^* = \frac{P^*}{\phi_1 P_1^*/T_1^* + \phi_2 P_2^*/T_2^*} \tag{5}$$

and $\tilde{v}$ for the mixture can be obtained from

$$\tilde{v}^{1/3} = \frac{1}{1 - \tilde{T}\tilde{v}/(1 + \tilde{P}\tilde{v}^2)} \tag{6}$$

In eq 4 the value of the contact energy interaction parameter, X_{12}, can be obtained in a number of ways.[18] Values for the mixtures used in this paper are obtained from the heat of mixing measurement of low molecular mass analogue materials.

Knowing these quantities for the pure components and their blends at atmospheric pressures, one can simulate the phase diagrams of mixtures as follows:

By definition at the binodal curve the two coexistent phases A and B are at chemical equilibrium where

$$(\Delta\mu_1)_A = (\Delta\mu_1)_B \tag{7a}$$

$$(\Delta\mu_2)_A = (\Delta\mu_2)_B \tag{7b}$$

where $\Delta\mu_i = \Delta\mu_i(\text{combinatorial}) + \Delta\mu_i(\text{residual})$. In a system with LCST behavior, as the temperature increases the mixture becomes more unstable whereas in systems with UCST behavior, as temperature decreases the mixture becomes more unstable. The limit of this metastability is called the spinodal and is given by

$$\frac{\partial^2 \Delta G_M}{\partial \phi_2^2} = \frac{\partial \Delta\mu_i}{\partial \phi_i} = 0 \tag{8}$$

where ΔG_M is the Gibbs free energy change on mixing, given by

$$\Delta G_M = \Delta H_M - T[\Delta S_M(\text{residual}) + \Delta S_M(\text{combinatorial})] \tag{9}$$

Using the combinatorial entropy of mixing given by the classical Flory–Huggins theory and the residual quantities from the equation-of-state theory of Flory and co-workers,[1-4] one calculates ΔG_M as

$$\Delta G_M = \bar{r}Nv^*[\phi_1 P_1^*/\tilde{v}_1 + \phi_2 P_2^*/\tilde{v}_2 - P^*/\tilde{v}] + 3\bar{r}Nv^*\left[\phi_1 P_1^* \tilde{T}_1 \ln \frac{\tilde{v}_1^{1/3} - 1}{\tilde{v}^{1/3} - 1} + \phi_2 P_2^* \tilde{T}_2 \ln \frac{\tilde{v}_2^{1/3} - 1}{\tilde{v}^{1/3} - 1} - \frac{1}{3}\phi_1\theta_2 T Q_{12} \right] + RT[n_1 \ln \phi_1 + n_2 \ln \phi_2] \tag{10}$$

The chemical potential of component 1 in the mixture relative to pure component is defined as

$$\mu_1 - \mu_1^\circ = \left(\frac{\partial \Delta G_M}{\partial N_1}\right)_{T,V_1,N_2} + \left(\frac{\partial \Delta G_M}{\partial \tilde{v}}\right)_{T,N_1,N_2}\left(\frac{\partial \tilde{v}}{\partial N_1}\right)_{T,V,N_2} = RT\left[\ln \phi_1 + \left(1 - \frac{r_1}{r_2}\right)\phi_2 \right] + P_1^* V_1^* \left\{ 3\tilde{T}_1 \ln \frac{\tilde{v}_1^{1/3} - 1}{\tilde{v}^{1/3} - 1} + \tilde{v}_1^{-1} - \tilde{v}^{-1} + \tilde{P}_1(\tilde{v} - \tilde{v}_1) \right\} + \frac{V_1^* \theta_2^2}{\tilde{v}}(X_{12} - T\tilde{v}Q_{12}) \tag{11}$$

and similarly that for component 2 in the mixture is

$$\mu_2 - \mu_2^\circ = RT\left[\ln \phi_2 + \left(1 - \frac{r_2}{r_1}\right)\phi_1 \right] + P_2^* V_2^* \left\{ 3\tilde{T}_2 \ln \frac{\tilde{v}_2^{1/3} - 1}{\tilde{v}^{1/3} - 1} + \tilde{v}_2^{-1} - \tilde{v}^{-1} + \tilde{P}_2(\tilde{v} - \tilde{v}_2) \right\} + \frac{V_2^* \theta_1^2}{\tilde{v}} \frac{s_2}{s_1}(X_{12} - T\tilde{v}Q_{12}) \tag{12}$$

Equations 11 and 12 and the binodal condition can be used to compute the position of the binodal curve. To simulate the binodal curve we used a search procedure whereby positions of equal chemical potential of component 1 are found and then the minimum differences between the chemical potentials of component 2 over these compositions are found.

The spinodal curve can be simulated directly by differentiating either eq 11 or 12 as we have shown elsewhere[7-9] or can alternatively be found from the maxima and minima of $\Delta\mu_i$ while carrying out the search procedure for the binodal. The two procedures give identical results.

A similar treatment for the simulation of the binodal and spinodal was applied at elevated pressures by using constant values of T^*, P^*, and V^* and neglecting the effect of pressure on X_{12} and Q_{12} as explained earlier.

Results and Discussion

1. Mixtures of Oligomeric Polystyrene and Polybutadiene. The molecular mass, molecular mass distributions, and state parameters of the two polybutadiene and three polystyrene oligomers used in this work are given in Table I. The density and thermal expansion coefficients of polybutadiene were obtained from ref 11. Those of polystyrene were calculated by using equations obtained from the literature.[15] The thermal pressure coefficients were estimated from their solubility parameter values obtained by the group contribution method.[16]

From a combination of these materials five quasi-binary mixtures were studied. The binary state parameters of these are given in Table II. The values of the contact interaction parameter, X_{12}, were obtained by fitting the experimental heat of mixing data to eq 4 with

$$\Delta H_M = \bar{r}Nv^*\{\phi_1 P_1^*/\tilde{v}_1 + \phi_2 P_2^*/\tilde{v}_2 - P^*/\tilde{v}\} \tag{13}$$

The values of the contact entropy parameter, Q_{12}, were adjusted to fit the minima of the phase diagrams to those of the corresponding cloud point curves at atmospheric pressure. The surface area per unit volume ratios were calculated by using Bondi's group contribution data.[17]

The resulting simulated phase diagrams are shown in Figures 1–5 along with the experimental cloud point measurements described elsewhere.[11] Only results at atmospheric pressure and at 1000 atm are presented but intermediate results show a comparable fit. No results are

Table I
Specifications of the Oligomeric Materials and Their State Parameters

notation	oligomer	$\bar{M}_n$	$\bar{M}_w/\bar{M}_n$	d,[a] g cm^{-3}	$\alpha \times 10^4$, K^{-1}	γ, J cm^{-3}
PEGM600	poly(ethylene glycol), methoxylated	600	1.10	1.0718	7.8	1.08
PPGM400	poly(propylene glycol), methoxylated	400	1.15	0.95694	8.7	0.85
PPGM1000	poly(propylene glycol), methoxylated	1000	1.07	0.97752	8.5	0.93
PPGM1500	poly(propylene glycol), methoxylated	1500	1.08	0.98522	8.3	0.93
PPGM2000	poly(propylene glycol), methoxylated	2000	1.10	0.98814	8.2	0.95
PBD920	polybutadiene	920	1.20	0.833	7.0	1.0
PBD2350	polybutadiene	2350	1.10	0.850	7.0	1.0
PS1200	polystyrene	1200	1.12	1.0277	6.3	1.1
PS1520	polystyrene	1520	1.10	1.046	6.2	1.1
PS3900	polystyrene	3900	1.12	1.020	5.8	1.1

[a] Data for PBD and PS are given at 25 °C and those for PEGM and PPGM at 30 °C.

Table II
Binary State Parameters of Oligomeric Mixtures

no.	mixture	X_{12},[a] J cm^{-3}	Q_{12}, J cm^{-3} K^{-1}	S_2/S_1
1	PBD920–PS1200	7.0	0.0047	0.9
2	PBD920–PS1520	7.0	0.0063	0.9
3	PBD920–PS3900	7.0	0.0069	0.9
4	PBD2350–PS1200	7.0	0.0062	0.9
5	PBD2350–PS1520	7.0	0.0074	0.9
6	PEGM600–PPGM400	13.17	0	1.05
7	PEGM600–PPGM1000	13.17	0.0119	1.06
8	PEGM600–PPGM1500	11.65	0.0119	1.075
9	PEGM600–PPGM2000	10.64	0.0113	1.082

[a] 1 atm = 0.101325 J cm^{-3}. The X_{12} values of PBD–PS mixtures are given at 70 °C and those of PEGM–PPGM mixtures at 30 °C.

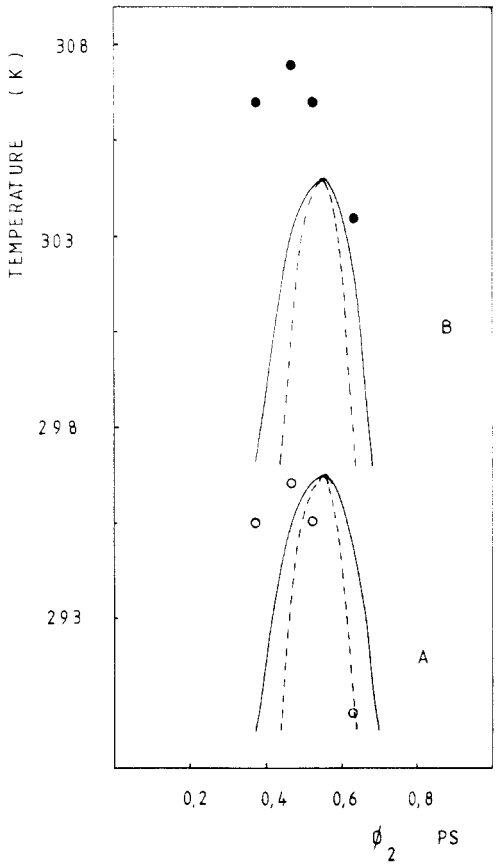

Figure 1. Simulated (—) binodals and (– – –) spinodals of PBD920–PS1200 mixtures at (A) 1 and (B) 1000 atm. The corresponding experimental cloud point data[11] at (○) 1 and (●) 1000 atm are also shown for comparison.

available for the highest molecular weight polystyrene with the highest molecular weight polybutadiene as this was not measured due to problems associated with the high viscosities.

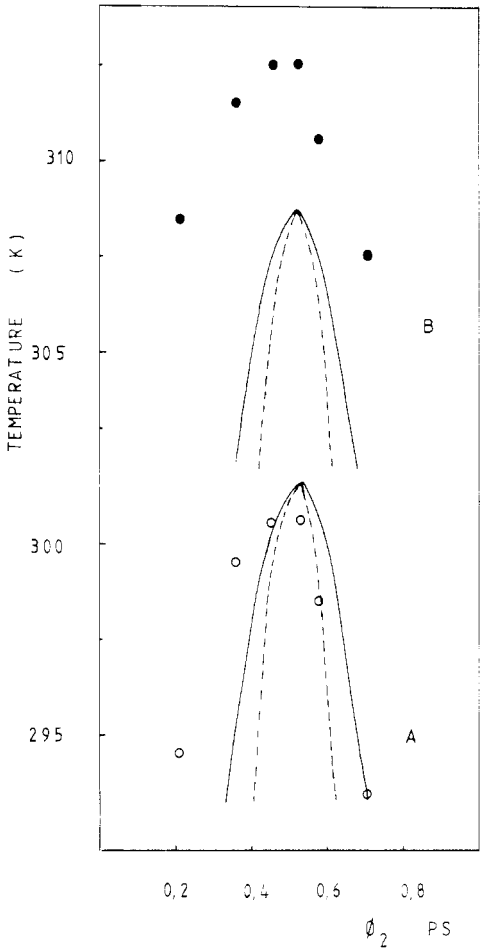

Figure 2. Simulated (—) binodals and (– – –) spinodals of PBD920–PS1500 mixtures at (A) 1 and (B) 1000 atm. The corresponding experimental cloud point data[11] at (○) 1 and (●) 1000 atm are also presented.

Table III
Theoretical and Experimental Values of $dT/dP \times 10^3$ for Oligomeric Mixtures

no.	mixture	$dT/dP \times 10^3$, K atm^{-1} theory	expt
1	PBD920–PS1200	7.7	11.0
2	PBD920–PS1520	7.0	12.0
3	PBD920–PS3900	8.0	15.1
4	PBD2350–PS1200	11.0	15.0
5	PBD2350–PS1520	10.0	13.0
6	PEGM600–PPGM400	10.0	9.0[a]
7	PEGM600–PPGM1000	10.4	11.0
8	PEGM600–PPGM1500	10.8	9.0
9	PEGM600–PPGM2000	10.0	8.0

[a] Taken at the same composition as the simulation since it is difficult to decide where the maximum occurs.

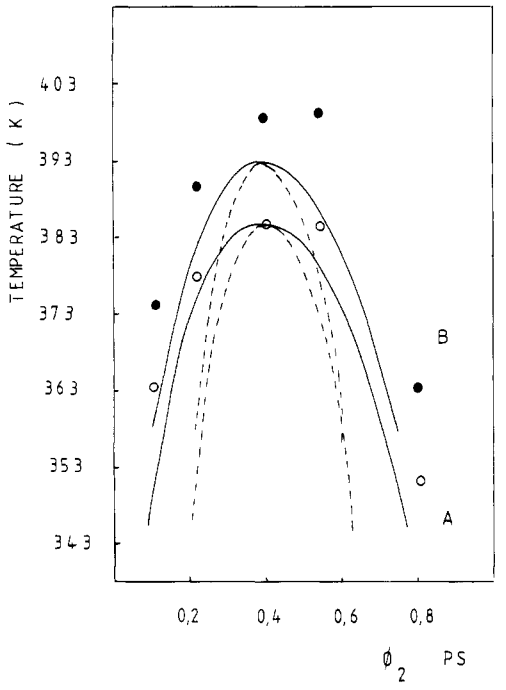

Figure 3. Simulated (—) binodals and (---) spinodals of PBD920–PS3900 mixtures at (A) 1 and (B) 1000 atm for the data of Tables I and II. The cloud point data[11] at (○) 1 and (●) 1000 atm are also shown.

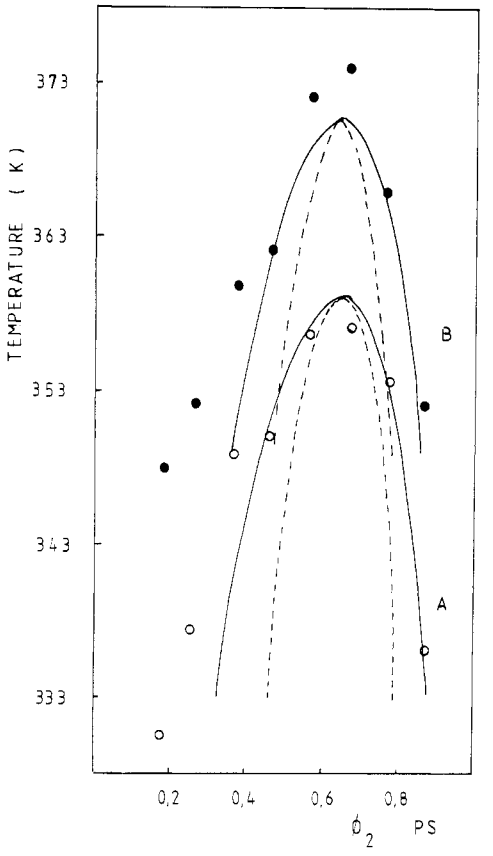

Figure 4. Theoretically simulated (—) binodals and (---) spinodals of PBD2350–PS1200 mixtures at (A) 1 and (B) 1000 atm. The cloud point data[11] of the mixtures at (○) 1 and (●) 1000 atm are also shown.

The theoretical and experimental values of dT/dP, the change in temperature of the cloud point per unit change in pressure, for the mixtures are collected in Table III. The quoted values correspond to the maximum of the simulated phase diagrams and that of the cloud point

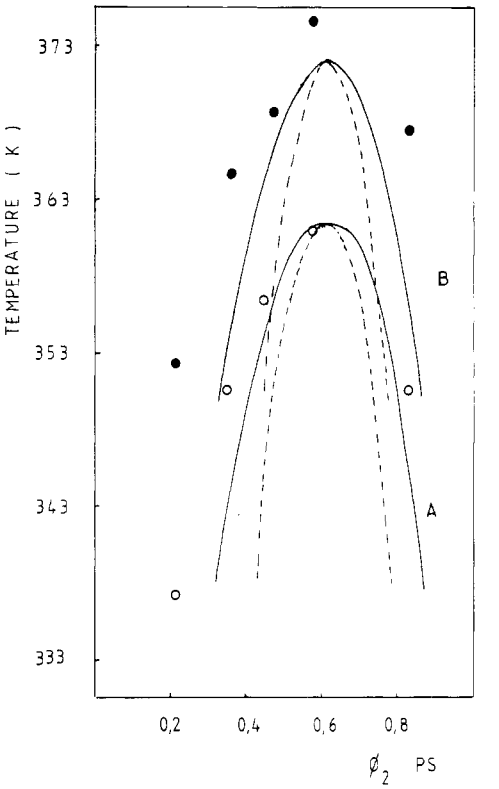

Figure 5. Simulated (—) binodals and (---) spinodals of PBD2350–PS1520 mixtures at (A) 1 and (B) 1000 atm. The cloud point data[11] at (○) 1 and (●) 1000 atm are also shown.

curves, respectively. Theoretical values of dT/dP are generally lower, being of the order of 70% of the experimental values. This could be due in part to experimental errors in measuring the cloud points or to uncertainties in the various state parameters used.

The shapes of the simulated phase diagrams are not identical with that of the measured cloud point curves but the fit is quite good considering the approximations used. The fit could be inproved by the adjustment of the various state parameters as has been desdribed elsehwere,[18] but there is little justification for this as the fit is already satisfactory.

A comparison of the data in Table II shows that, for a constant value of X_{12}, as the molecular masses of the polymers increases, the values of Q_{12} required to fit the simulation to the cloud point curve increase. This could be a result of errors in the various parameters such as the molecular masses of the polymers or to a molecular mass dependence of X_{12}. It could also be a real effect due to differences in ordering of the pure components and the mixtures at various molecular masses as has been found in mixtures of other substances.[19]

One can generally conclude that for these mixtures the theory gives a good representation both of the phase behavior at atmospheric pressure and of the effect of pressure.

2. Mixtures of Oligomeric, Methoxylated Poly(ethylene oxide) and Poly(propylene oxide). The pure component and binary state parameters of the poly(ethylene oxide), four different molecular mass samples of poly(propylene oxide), and four mixtures derived from then are given in Tables I and II. Due to the large chemical difference of the end groups from the main chain it was necessary to calculate values of the thermal pressure coefficients, γ, the contact interaction energies, X_{12}, and the surface area per unit volume ratios, S_2/S_1, individually. The resulting simulated phase diagrams at 1 and 1000 atm

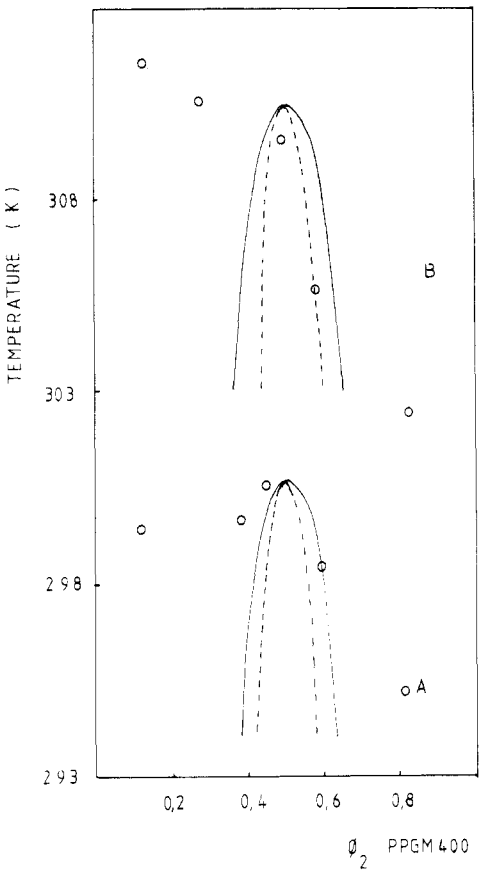

Figure 6. Simulated (—) binodals and (– – –) spinodals of PEGM600–PPGM400 mixtures at (A) 1 and (B) 1000 atm. The experimental cloud point data[11] (○) 1 and (●) 1000 atm are also shown.

Table IV
State Parameters for the Pure Polymeric Materials

material	$\alpha \times 10^4$, K^{-1}	γ, J cm^{-3} K^{-1}	v_{sp}, cm^3 g^{-1}	$\bar{M}_w \times 10^{-5}$ [a]
EVA45	4.5103	0.8045	1.0636	2.56
H48	4.4199	0.9544	0.81506	1.82
CPE3	3.6546	0.9592	0.8089	1.2
PES	2.0	1.5	0.7934	0.2
PEO	5.5	1.2	0.9183	0.2

[a] Relative to polystyrene by GPC.

are shown in Figures 6–9 along with the experimental cloud point data.

The values of dT/dP are again collated in Table III. It can be seen that the theoretical and experimental values of this quantity agree quite well. The shapes of the phase diagrams are, however, badly mismatched both at low and at high pressure. It should be noted that a measurement of the effect of pressure on the phase diagram is a very selective probe. The effect is predominantly due to the volume change on mixing and the equation-of-state terms in the free energy equation associated with this change. The fact that the theory satisfactorily predicts the value of dT/dP suggests that the theory does estimate the effect of the free volume changes correctly. The fact that the theory does not predict correctly the shape of the curve at any pressure suggests a composition, molecular mass, or system dependence of the interaction terms due to specific effects. The values of Q_{12} used in these simulations are approximately the same except in the case of the blend involving the lowest molecular mass poly(propylene oxide). This could be due to an error in the molecular mass of this oligomer. The higher molecular masses of poly(propylene oxide) have an improved general agreement between the theoretical predictions and experimental findings. The movement of the theoretical phase diagrams to the left with increased molecular weight can easily be explained in simple Flory–Huggins terms.[21]

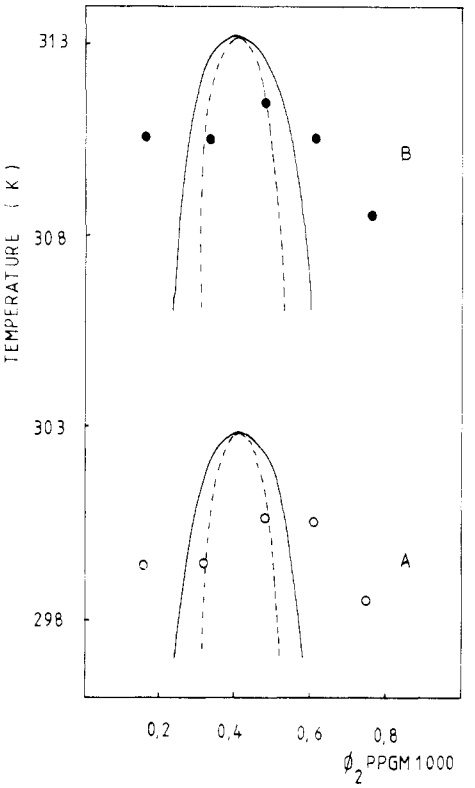

Figure 7. Simulated (—) binodals and (– – –) spinodals of PEGM600–PPGM1000 mixtures at (A) 1 and (B) 1000 atm. The corresponding experimental cloud point data[11] at (○) 1 and (●) 1000 atm are also shown.

The phase diagrams of these mixtures at atmospheric pressure have previously been reported by others elsewhere.[20] The slightly different values of the parameters used in our simulation are due to the fact that we have used the weight-average molecular masses instead of the number averages.

3. Mixtures of High Molecular Mass Polymers. The effect of pressure on the theoretical spinodal curve of high-polymer mixtures, calculated from the spinodal equation, has already been described in a previous publication.[13] In this paper we merely add to this a simulation of the binodal curves and use the results to compare with the oligomer mixtures discussed in the previous sections.

The pure component and binary state parameters of the polymers are given in Tables IV and V; the justification

Table V
Binary Parameters of Polymeric Mixtures

no.	mixture	X_{12}, J cm^{-3}	Q_{12}, J cm^{-3} K^{-1}	S_2/S_1	dT/dP, K atm^{-1} theory	dT/dP, K atm^{-1} expt
1	EVA45–CPE	−3.2	−0.00626	1.03	0.022	0.020
2	EVA45–H48	−2.63	−0.00676	0.98	0.010	0.014
3	PES–PEO	−40.0	−0.0482	1.2	0.044	0.046

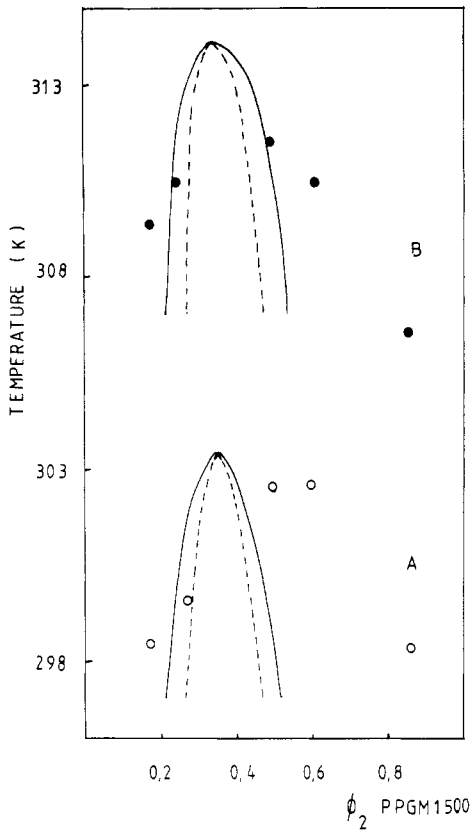

Figure 8. Simulated (—) binodals and (---) spinodals of PEGM600–PPGM1500 mixtures at (A) 1 and (B) 1000 atm. The cloud point data[11] at (○) 1 and (●) 1000 atm are also shown.

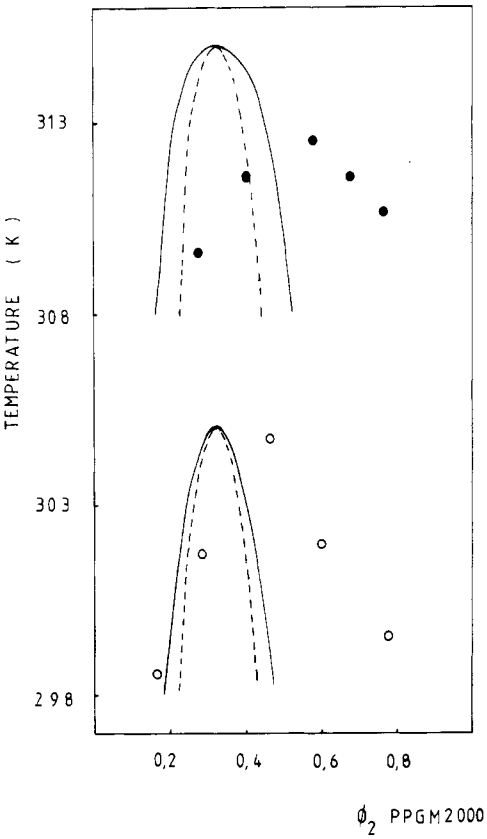

Figure 9. Simulated (—) binodals and (---) spinodals of PEGM600–PPGM2000 mixtures at (A) 1 and (B) 1000 atm. The cloud point data[11] at (○) 1 and (●) 1000 atm are also shown.

for and the procedure used in obtaining these values has been described previously.[6-9,13]

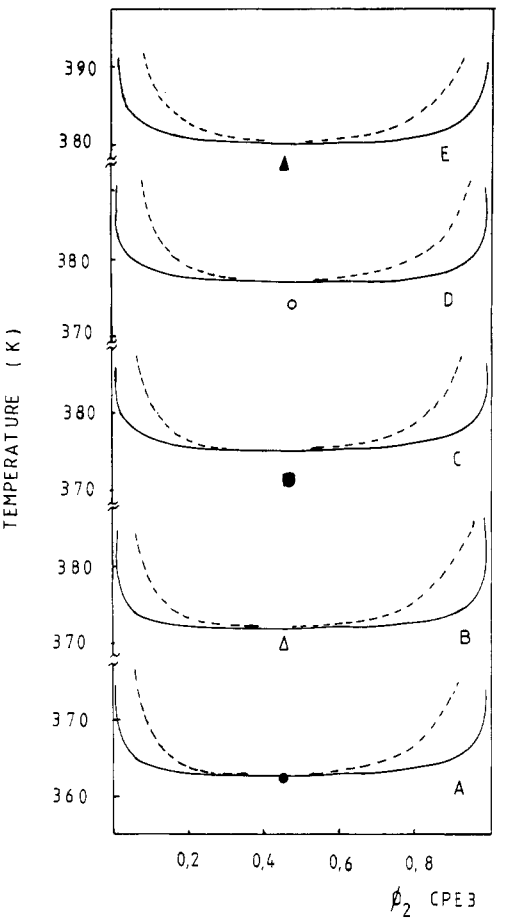

Figure 10. Simulated (—) binodals and (---) spinodals of EVA45–CPE3 mixtures. Experimental cloud point data at (A) 1 atm (●), (B) 300 atm (△), (C) 450 atm (■), (D) 550 atm (○), and (E) 750 atm (▲) are also shown.

The simulated spinodal and the binodal curves for mixtures of ethylene–vinyl acetate copolymer (45 wt % acetate content, EVA45) and chlorinated polyethylene (53 wt % Cl content, CPD3) at various pressures are shown in Figure 10. Similar results for mixtures of EVA45 and chlorinated polyethylene (43 wt % Cl content, H48) at the given pressures are shown in Figure 11. The simulated phase diagrams of polyether sulfone (PES) with poly(ethylene oxide) (PEO) at several pressures are shown in Figure 12. The experimental cloud point data of these mixtures are also presented for comparison.

As is shown in these figures the shape of the phase diagrams does not change with increasing pressure. The flatness of the curves is mainly due to the large values of X_{12}, which were obtained from heat of mixing measurements using analogue materials.

Application of pressure on blends of these mixtures has increased the miscibility, giving positive values of dT/dP as is shown in Table V. The calculated values of the volume change on mixing of these mixtures using the values of dT/dP are given elsewhere.[13] When comparing these results with those of oligomer mixtures, one should bear in mind that in the latter the cloud point curve probably corresponds fairly closely to the binodal curve whereas for the high-polymer mixtures it may correspond more closely to the spinodal. Much of the phase diagrm in the high-polymer mixtures is inaccessible due to instrumental limitations and thus it has not been possible to explore the shape of these curves, especially at higher pressures. One can thus only make conclusions concerning the movement with pressure close to the minimum of the cloud point curves.

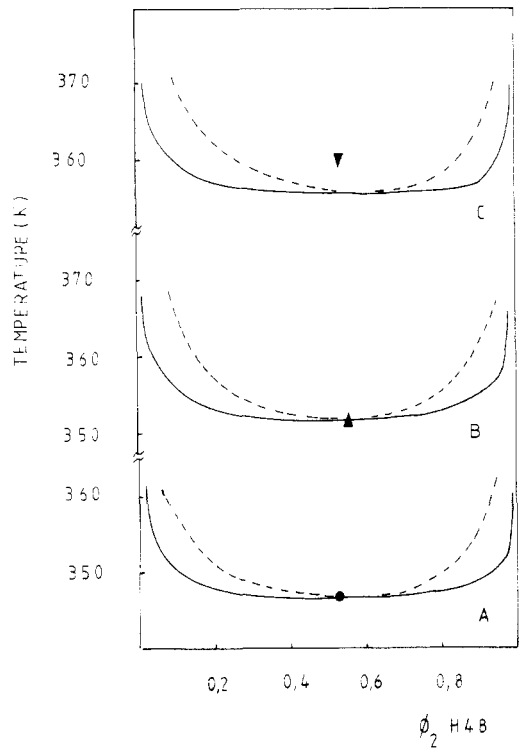

Figure 11. Simulated (—) binodals and (---) spinodals and measured cloud point data of EVA45–H48 mixtures. Experimental cloud point data at (A) 1 atm (●), (B) 300 atm (▲), and (C) 858 atm (▼) are also shown.

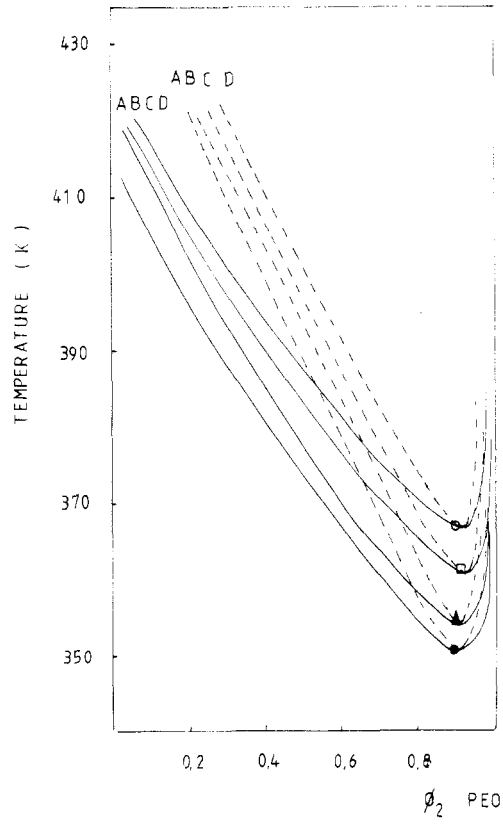

Figure 12. Simulated (—) binodals and (---) spinodals and measured cloud points for PES–PEO mixtures at (A) 1 atm (●), (B) 108 atm (▲), (C) 221 atm (□), and (D) 348 atm (○).

The contact entropy parameter, Q_{12}, is the only adjustable parameter used in all these simulations. It is found to be negative for mixtures of high polymers with negative heats of mixing and positive for oligomer mixtures with positive heats of mixing. It is apparent that the equation-of-state theory is successful in predicting the sign and magnitude of the pressure effect for high-polymer mixtures as well as oligomer mixtures.

Conclusion

The equation-of-state theory of Flory and co-workers has been satisfactorily used to simulate the binodal and spinodal curves of oligomer–oligomer and polymer–polymer mixtures at various pressures. The application of pressure on mixtures with negative heats of mixing is predicted to increase the miscibility, whereas it is predicted to decrease the miscibility of mixtures with positive heats of mixing. This is in accord with experimental findings.

Acknowledgment. We thank Sir Geoffrey Allen for useful discussion and acknowledge the work of the late J. B. P. Tripathi, whose unpublished results, while working with Sir Geoffrey Allen, form the basis of this work.

Appendix. List of Symbols Used

d	density
ΔG_M	free energy of mixing
ΔH	enthalpy of mixing
P	pressure
$\tilde{P}_i$	reduced pressure of species i
P_i^*	hard-core pressure of species i
$\tilde{P}$	reduced pressure of mixture
P^*	hard-core pressure of mixture
Q_{12}	contact entropy parameter
$\bar{r}N$	average number of segments in the mixture
R	gas constant
r_i	chain length of molecule i
S_i	number of contact sites per segment in species i
ΔS_M	entropy of mixing
T	temperature
$\tilde{T}_i$	reduced temperature of species i
T_i^*	hard-core temperature of species i
$\tilde{T}$	reduced temperature of mixture
T^*	hard-core temperature of mixture
V_1^*	molar hard-core volume of component 1
v_{sp}	specific volume of component i
$\tilde{v}_i$	reduced volume of component i
v_i^*	hard-core volume of component i
$\tilde{v}$	reduced volume of mixture
v^*	hard-core volume of mixture
X_{12}	contact interaction parameter
α	thermal expansion coefficient
γ	thermal pressure coefficient
ϕ_i	segment fraction of species i
θ_i	site fraction of species i
$\Delta\mu_i$	chemical potential of component i

References and Notes

(1) Flory, P. J. *J. Am. Chem. Soc.* **1965**, *87*, 1833.
(2) Abe, A.; Flory, P. J. *J. Am. Chem. Soc.* **1966**, *88*, 2887.
(3) Flory, P. J.; Orwell, R. A.; Vrij, A. *J. Am. Chem. Soc.* **1964**, *86*, 3567.
(4) Eichinger, B. E.; Flory, P. J. *Trans. Faraday Soc.* **1968**, *65*, 2035.
(5) McMaster, L. *Macromolecules* **1973**, *6*, 760.
(6) Chai, Z.; Ruona, S.; Walsh, D. J.; Higgins, J. S. *Polymer* **1983**, *24*, 263.
(7) Rostami, S.; Walsh, D. J. *Macromolecules* **1984**, *17*, 315.
(8) Walsh, D. J.; Rostami, S.; Singh, V. B. *Makromol. Chem.* **1985**, *186*, 145.
(9) Walsh, D. J.; Rostami, S. *Polymer*, in press.
(10) Saeki, S.; Kuwahara, N.; Konno, S.; Kaneko, M. *Polymer* **1983**, *16*, 388.
(11) Tripathi, J. B. P. Ph.D. Thesis, Imperial College, 1979.
(12) Wolf, A. B.; Blaum, G. *J. Polym. Sci. Polym. Symp.* **1977**, *No. 61*, 25.
(13) Walsh, D. J.; Rostami, S. *Macromolecules* **1985**, *18*, 216.

(14) Schoen, P. E.; Priest, R. G.; Sheridan, J. P.; Schmur, J. M. J. Chem. Phys. 1979, 71, 317.
(15) Richardson, M. J.; Saville, N. G. Polymer 1977, 18, 3.
(16) Hoy, K. L.; J. Paint Technol. 1970, 42, 76.
(17) Bondi, A. J. Phys. Chem. 1964, 68, 441.
(18) Walsh, D. J.; Rostami, S. Adv. Polym. Sci., in press.
(19) Tancrede, P.; Patterson, D.; Botharel, P. J. Chem. Soc., Faraday Trans. 2 1977, 73, 29.
(20) Allen, G.; Chai, Z.; Chong, C. L.; Higgins, J. S.; Tripathi, J. B. P. Polymer 1984, 25, 239.
(21) Flory, P. J. "Principles of Polymer Chemistry"; Cornell University Press: Ithaca, NY, 1953.

Heat of Formation of Poly(4-methylpentene-1) Gels

H. Phuong-Nguyen and G. Delmas*

Chemistry Department, Université du Quebec à Montréal, Montréal C.P. 8888, H3C 3P8 Canada. *Received March 26, 1984*

ABSTRACT: Heats of gel formation have been measured for poly(4-methylpentene-1) (P4MP1) gels, in order to investigate the molecular origin of their cohesive junctions. The latter, which were previously found to be noncrystalline, are stable in cyclopentane (c-C_5) and cyclohexane (c-C_6) more than 50 °C above the dissolution temperature T_D of the chain-folded crystals. Heats have been measured between 25 and 75 °C below or above T_D depending on the solvent. Below T_D, at 25 °C, the heats (in this case, heats of swelling) have been obtained in linear, branched, and cyclic alkanes. Above T_D, the polymer–solvent interacting parameter in solution, h^E(interaction), can be calculated. For $\phi_p < 0.02$ the final state is a pseudosolution containing aggregates, while for $\phi_p > 0.02$ it is a gel. The main features are the following: (1) h^E(interaction) is *exothermic* and can be almost as large as the endothermic heat of fusion. (2) h^E(interaction) is concentration dependent, reaching a plateau for $\phi_p = 0.20$. (3) A sharp variation of h^E(interaction) is noted when the final state changes from a solution to a gel. (4) h^E(interaction) diminishes when T increases and extrapolates to 0 at the gel–solution transition (110 °C). The sign of h^E(interaction) and its variation with ϕ_p are characteristic of an association between the polymer chains either in the pseudosolution or in the gel. These results support the previously proposed model of junctions consisting of cohesive associations of regularly spiraled helices, stabilized by solvent.

Introduction

Thermoreversible gels may exist in nonpolar systems if the macromolecule has a "copolymeric" character due to differences in chemical nature or stereoregularity. This allows the cohesive regions to coexist in the solvent with the solution-like regions of random coils which give the gel its elasticity. The participation of the same chain in successive ordered and disordered regions is a requirement of the gel state.[1]

During the last decade, the conditions required for forming gels from solutions of several isotactic polymers have been discovered, initiating a surge of effort toward the understanding of their molecular origin. It is generally proposed that gelation is due to different modes of crystallization of the same chains in a given solvent—namely, fringed micellar crystallization, responsible for the cohesive regions, and the usual chain-folding crystallization. A gel is formed if, under special conditions of solvent quality, temperature, and thermal history, fringed micellar crystals are present and stable—but not chain-folded crystals. If gels of stereoregular polymers share the common feature of being quite unexpected, the prerequisites for their occurrence are varied, involving either stirring, quenching at high supercooling, or changing the solvent quality. Recent investigations have revealed new features related to conformation of the chain (isotactic polystyrene (iPS)[2-4]), polymer crystallizability (polyethylene (PE),[5] poly(vinyl chloride) (PVC),[6] poly(*p*-chlorostyrene) (PCS)[7]), and effect of molecular weight and stirring on gelation (PE and polypropylene (PP)[8]). Gels of atactic polystyrene have also been investigated.[9]

This work, which follows a previous one[10] on the characterization of gels of a highly isotactic branched polyolefin, poly(4-methylpentene-1) (P4MP1), investigates the nature of the cohesive junctions through measuring the heat of formation of the gels.

Characteristic Features of P4MP1 Gels. P4MP1 has been studied[11] both in its nascent state (sample N) and after slow recrystallization from the melt (sample M). At the dissolution temperature of the chain-folded crystals, T_D, sample M forms a solution, while sample N experiences gelation at polymer volume fractions higher than about 0.02. However, the M solutions turn to clear gels on isothermal standing at higher temperature than the crystallization temperature of the chain-folded crystals. P4MP1 gels exhibit high thermal stability, since the gel–solution transition (or solation) temperature, T_S, is observed in cyclopentane and cyclohexane at 110 °C, well above the solvent boiling point. The results are consistent with the existence in N, but not in M, of a certain organization which is, in turn, the precursor of network junctions. In a solvent, the junctions can be destroyed by raising the temperature and re-formed on cooling after a suitable thermal history. With enough time, the polymer chains in the solutions of sample M can acquire the necessary characteristics to form a gel. If so, they also acquire the organization precursor of the gel since the polymer sample obtained after drying the gel again gives a gel at the dissolution temperature, as does sample N.

P4MP1 Solutions. Dilute-solution properties at high temperature in good solvents have indicated that the P4MP1 molecules are in the expected statistical coil conformation.[12] In cycloalkanes, on the other hand, solutions of this highly crystalline polymer (T(fusion) = 240 °C) are stable below 100 °C, even as low as room temperature in c-C_5. The solutions are actually pseudosolutions containing aggregates which display high intrinsic viscosities. In c-C_6, the disappearance of the aggregates when the temperature increases has been followed by measurements of intrinsic viscosities. The latter diminishes abruptly from about 8 to 0.8 dL g^{-1} at 98 °C but it is a slow process which takes several days.[10]

Nature of the Junctions. Since neither a sizable X-ray crystallinity of the gels between T_D and T_S nor any heat effect at T_S can be detected, the junctions in P4MP1 gels are unlikely to be fringed micellar crystals. If the inherent high cohesion of crystals is not at the origin of the junctions, the cohesion in the gels could originate from a

0024-9297/85/2218-1235$01.50/0